Atmos. Chem. Phys. Discuss., doi:10.5194/acp-2017-344, 2017
Manuscript under review for journal Atmos. Chem. Phys.
Discussion started: 26 April 2017

Atmospheric Chemistry and Physics Discussions

What controls the seasonal cycle of columnar methane observed by GOSAT over different regions in India?

Naveen Chandra[1*], Sachiko Hayashida[1], Tazu Saeki[2], and Prabir K. Patra[2]

[1] Nara Women's University, Kita-Uoya Nishimachi, Nara 630-8506, Japan
[2] Department of Environmental Geochemical Cycle Research, JAMSTEC, Yokohama 2360001, Japan

Correspondence to: Naveen Chandra (nav.phy09@gmail.com)

Abstract. Methane (CH_4) is one of the most important short-lived climate forcer (SLCFs) according to the United Nations Environment Programme as well as it plays also a critical role in air pollution chemistry in the troposphere. With the availability of satellite observations from space, variabilities in CH_4 have been captured for most parts of the global land with major emissions. The satellite observations however do not allow us to derive emission information straightforwardly, unlike in-situ measurements near the source region, without separating the role of transport and chemistry in the columnar dry-air mole fractions of methane (XCH_4), which involves the CH_4 densities at all altitudes along the solar light path. Observations of enhanced XCH_4 are often linked to the local/regional emissions by simple correlation, without separating transport and chemistry contributions to XCH_4 variability. Here, we present the analysis of XCH_4 variability over different inland and surrounding cleaner oceanic regions of India using GHGs Observation SATellite (GOSAT). We also use the JAMSTEC's state-of-the-art atmospheric chemistry-transport model (ACTM) for simulating the observed XCH_4 concentrations by varying surface emissions. The model-observation comparisons help us to elucidate the synoptic and seasonal variabilities in XCH_4 in relation with coupled monsoon meteorology and surface fluxes. Distinct seasonal variations of XCH_4 have been observed over the regions lying in the northern (north of 15°N) and southern part (south of 15°N) of India, corresponding to the peak during southwest (SW) monsoon (July-September) and early autumn season (October-December), respectively. The detailed study of all possible governing factors (transport, emission and chemistry) responsible for XCH_4 seasonal cycle suggests that distinct XCH_4 seasonal cycle over northern and southern regions of India is not only governed by the heterogeneous distributions of surface emissions, but also distribution of CH_4 in the upper tropospheric layer. We have observed different contributions from lower troposphere (~1000-600 hPa), affected mainly by surface emissions, and transport dominated upper atmosphere (~600-0 hPa) in the XCH_4 seasonal cycle. Over most of northern part of the Indian regions, up to 40% of the peak during the SW monsoon season is attributed to the lower troposphere, while ~60% to uplifted high-CH_4 air masses in the upper atmosphere. In contrast, XCH_4 enhancement over the semi-arid western India is mainly (~88%) attributed to the upper atmosphere. The ratios of contribution changed over the southern peninsula and cleaner oceanic region; up to 60% of seasonal cycle of XCH_4 is contributed by lower tropospheric region. These

Atmos. Chem. Phys. Discuss., doi:10.5194/acp-2017-344, 2017
Manuscript under review for journal Atmos. Chem. Phys.
Discussion started: 26 April 2017

Atmospheric Chemistry and Physics Discussions

differences arise due to the complex atmospheric transport mechanisms, caused by the seasonally varying monsoon. The CH_4 enriched air masses uplifted from high emission region by the SW monsoon circulation and deep cumulus convection, and then confined by anticyclonic wind in the upper troposphere (~200 hPa), cause the strong contribution of the upper troposphere in the peak of XCH_4 over most of the regions lying in the northern part of India. Based on this analysis, we suggest that a link between surface emissions and higher levels of XCH_4 is not always valid over Asian monsoon regions, although there is often a fair correlation between surface emissions and XCH_4.

1. Introduction

Methane (CH_4) is the second most important anthropogenic greenhouse gas (GHG) after carbon dioxide (CO_2) and accounts for ~20% (+0.97 W m^{-2}) of the increase in total direct radiative forcing, since 1750 (Myhre et al., 2013). CH_4 is emitted from a range of anthropogenic and natural sources in the atmosphere. The main natural sources of CH_4 include wetlands and termites (Cao et al., 1998; Sugimoto et al., 1998). Livestock, rice cultivation, fossil fuel industry (production and uses of natural gas, oil and coal) and landfills are the major sectors among the anthropogenic sources (Crutzen et al., 1986; Minami and Neue, 1994, Olivier et al., 2006; EDGAR2FT, 2013).

With a short atmospheric lifetime of about 10 years (e.g., Patra et al., 2011) and having 34 times more potential to trap heat than CO_2 on per molecule basis over a 100-year timescale, mitigation of CH_4 emissions could be the most important way to limit global warming at inter-decadal time scales (Shindell et al., 2009). Better knowledge of CH_4 distribution and quantification of its emission flux is indispensable for assessing possible mitigation strategies. However, sources of CH_4 are not yet well quantified due to sparse ground based measurements, which results in limited representation on a larger scale (Dlugokencky et al., 2011; Patra et al., 2016). Recent technological advances have made it possible to detect spatial and temporal variations in atmospheric CH_4 from space (Frankenberg et al., 2005; Kuze et al., 2009), which could fill in gap left by ground-based measurements, albeit at a lower accuracy than *in situ* measurements. Although satellite observations have the advantage of providing continuous monitoring over a wide spatial range, the information obtained from passive nadir-sensors, which use solar radiation at Short-Wavelength Infrared (SWIR) spectral region, is limited to XCH_4. This is an integrated measure of CH_4 with contributions from the different vertical atmospheric layers, i.e., from the Earth's surface to the top of the atmosphere (up to about 100km).

The Indian region exerts a significant impact on the global CH_4 emissions. The Indo-Gangetic Plane (IGP), mostly hot and humid northeast region lies in the foothills of the Himalayas, is one of the most polluted regions in the world due to the high population density, heavy industries, power plants that host 70% of coal-fired thermal power plants in India and intense agricultural activity (Kar et al., 2010). It is well known from previous studies that southwest (SW) monsoon (July-September) meteorology affects significantly the pollutants including CH_4 mixing ratios from surface to upper troposphere (400 – 200 hPa) (Park et al., 2004; Randel et al., 2006; Xiong et al., 2009; Baker et al., 2012; Schuck et al., 2012; Lal et al.,

2014, Chandra et al., 2016). Rain during the SW monsoon season cause higher CH_4 emissions from the paddies field and wetlands (e.g., Hayashida et al., 2013) while the persistent deep convection uplift the CH_4-laden air mass from surface to the upper troposphere during the same season (Baker et al., 2012; Schuck et al., 2012), where CH_4 is further spread over larger region by the anticyclonic winds. The dynamical system dominated by deep convection and anticyclone cover mostly the northern Indian region (north of 15°N) due to the presence of Himalayas and Tibetan Pleatu, while such complex dynamical system has not been observed over the southern part of India (south of 15°N) (Rao, 1976).

Satellite-based measurements show elevated levels of XCH_4 over the northern part of India (north of 15°N) particularly high over IGP during the southwest (SW) monsoon season (July to September) and over southern India (south of 15°N) during early autumn (October to December) season (Frankenberg et al., 2005, 2006; Hayashida et al., 2013). Previous studies related the high XCH_4 values correspond to the strong surface CH_4 emissions particularly from the rice cultivation over the Indian region, because they showed statistically significant correlations over certain regions (Hayashida et al., 2013; Kavitha et al., 2016). The differences in the peak of XCH_4 seasonal cycle over northern and southern regions of India are discussed on the basis of agricultural practice in India that takes place in two seasons, namely the Kharif (May to October) and Rabi (November to April), respectively. However, inferring the local emissions to the higher levels of XCH_4, which involves all of the CH_4 abundances at any altitude along the solar light path, is highly ambiguous, particularly over the regions where monsoon meteorology significantly affects the tropospheric distributions of CH_4 by coupling the surface emission to upper tropospheric air. Therefore, data indicating the vertical distributions of CH_4 are important when measurements of XCH_4 are used to investigate underlying surface emissions.

Although GOSAT has also a Thermal InfraRed (TIR) channel for providing the vertical distributions of CH_4, but the retrieval products are still under validation (e.g., Zou et al., 2016, Olsen et al., 2017). There are some other infrared sensors such as AIRS and TES, which could provide some information of vertical distributions of CH_4, but they are not sufficiently sensitive to the lower troposphere (approximately bias ~ 65 ppb) (Worden et al., 2015). Some studies have been done to discriminate lower tropospheric CH_4 from the upper part, but most of work is still under validation (e.g., Worden et al., 2015). Under the limitations of satellite in providing information on vertical CH_4 distributions, the Atmospheric Chemistry transport model (ACTM) becomes a powerful tool to understand its vertical distribution along with major controlling factors emissions, transport, and chemistry processes separately. This manuscript attempts for the first time to separate the factors responsible (emission, transport and chemistry) for the distributions of columnar methane (XCH_4) over the Asian monsoon region for different altitude segments. The XCH_4 mixing ratios, observed from the Greenhouse gases Observing SATellite (GOSAT) and simulated from JAMSTEC's ACTM, are used for this study. The main conclusion drawn from this study is that a link between surface emission seasonality and higher XCH_4 values over the Asian monsoon region is not always valid, although there is often a fair correlation between them. Transport dominated upper atmospheric layer contribute significantly in the higher levels of XCH4 during the seasons of high convective activity.

Atmos. Chem. Phys. Discuss., doi:10.5194/acp-2017-344, 2017
Manuscript under review for journal Atmos. Chem. Phys.
Discussion started: 26 April 2017

Atmospheric Chemistry and Physics Discussions

2. Methods

2.1 Satellite data:

The Greenhouse gases Observing SATellite (GOSAT) (called Ibuki) is a joint satellite project of National Institute of Environmental Studies (NIES), Ministry of the Environment (MOE) and Japan Aerospace Exploration Agency (JAXA). It has been providing global observations of columnar mixing ratios of greenhouse gases (XCH_4 and XCO_2) since its launch in January 2009. It is equipped with onboard thermal and near infrared sensors for carbon observations (TANSO), which include a Fourier transform spectrometer (FTS) for GHG's monitoring and a cloud and aerosol imager (CAI) to detect cloud and aerosols in the FTS field of view (Kuze et al., 2009). Cloudy data is strictly screened using simultaneously recorded atmospheric images from CAI. As a result of strict screening, only limited numbers of XCH_4 data are available during the SW monsoon season over South Asia. This study uses the GOSAT SWIR XCH_4 (Version 2.21)-Research Announcement product for the period of 2011-2014. GOSAT measurements are extensively validated using the ground-based measurements of XCH_4, obtained using the worldwide network of ground based Fourier Transform Spectrometer (FTS) called the Total Carbon Column Observing Network (TCCON). Retrieval bias and precision of column abundance from GOSAT SWIR observations have been estimated as approximately 15-20 ppb and 1%, respectively for the NIES product using TCCON data (Morino et al., 2011; Yoshida et al., 2013). The good precision and low bias of the GOSAT instrument assures high quality of XCH_4 data.

2.2. Model simulations

Model analysis is comprised of simulations from the well-established atmospheric general circulation model (AGCM)-based chemistry-transport model (ACTM; Patra et al., 2009). The AGCM was developed by the Center for Climate System Research/National Institute for Environmental Studies/Frontier Research Center for Global Change (CCSR/NIES/FRCGC). It has been a part of the chemistry-transport model inter-comparison experiment TransCom-CH_4 (Patra et al., 2011) and used in inverse modeling of CH_4 emissions (Patra et al., 2016). The ACTM runs at a horizontal resolution of T42 spectral truncations (~$2.8^O \times 2.8^O$) with 67 sigma-pressure vertical levels. The evolution of CH_4 at different longitude (x), latitude (y) and altitude (z) with time in the Earth's atmosphere depends on the surface emission, chemical loss and transport and mathematically can be represented by the following continuity equation:

$$\frac{dCH_4(x,y,z,t)}{dt} = S_{CH4}(x,y,t) - L_{CH4}(x,y,z,t) - \nabla.\phi(x,y,z,t)$$

where

CH_4 = methane molar fraction in the atmosphere

S_{CH4} = Total emissions/sinks of CH_4 at the surface

Atmos. Chem. Phys. Discuss., doi:10.5194/acp-2017-344, 2017
Manuscript under review for journal Atmos. Chem. Phys.
Discussion started: 26 April 2017

Atmospheric Chemistry and Physics Discussions

L_{CH4} = Total loss of CH_4 in the atmosphere due to the chemical reactions

$\nabla.\phi$ = Transport of CH_4 due to the advection, convection and diffusion.

The meteorological fields of ACTM are nudged with reanalysis data from the Japan Meteorological Agency, version JRA-25 (Onogi et al., 2007). The model uses an optimized OH field (Patra et al., 2014) based on a scaled version of the seasonally varying OH field (Spivakovsky et al., 2000). The a-priori anthropogenic emissions are from Emission Database for Global Atmospheric Research (EDGAR) v4.2 FT2010 database (http://edgar.jrc.ec.europa.eu). Two different emission scenarios (AGS and CTL) are used to examine model sensitivity to change in the underlying fluxes in simulations of the total atmospheric column and lower tropospheric column. First one is the ACTM_AGS, where all emission sectors in EDGAR42FT are kept at constant at a value for 2000, except for emissions from agriculture soils. The second one is controlled emission scenario referred by ACTM_CTL, which is based on the ensemble of the anthropogenic emissions from EDGAR32FT (as in Patra et al., 2011), wetland and biomass burning emissions from Fung et al (1991) and rice paddies emission from Yan et al (2009). Further details about the model and these emission scenarios can be found in the previous studies (Patra et al., 2009; Patra et al., 2011; Patra et al., 2016). XCH_4 is calculated from the ACTM profile using the following formula.

$$XCH_4 = \Sigma_{n=2}^{60} CH_4(n) * [(\sigma_p(n) + \sigma_p(n-1))/2 - (\sigma_p(n) + \sigma_p(n+1))/2]$$

For the first layer (n =1)

$$XCH_4 = \Sigma_{n=1} CH_4(n) * [1 - (\sigma_p(n) + \sigma_p(n+1))/2]$$

where

n = number of vertical sigma pressure layer,

σ_p = sigma pressure level and

One simple approach i.e. the seasonal distributions of partial columnar CH_4 (denoted by X_pCH_4) at a difference of 0.2 sigma pressure layers using the same formula, is used to understand the contribution of different layers in the XCH_4 seasonal cycle. Because the averaging kernels (AKs) are nearly uniform in the troposphere (Yoshida et al., 2013), this approximation does not lead to serious errors in constructing XCH_4 and X_pCH_4 in the tropical region; our study is further limited to the Indian subcontinent only. For both the CTL and AGS cases, we adjust a constant offset of 20 ppb to the modeled time series, which should make the *a priori* correction have a lesser impact on the model XCH_4. Because the focus of this study is seasonal and spatial variations in XCH_4, a constant offset adjustment should not affect the main conclusions. XCH_4 data are sampled at the nearest model grid from the available observations and satellite overpass time (~ 1300 hrs LT) and then averaged over the selected partitions of the study region (Figure 2a).

Atmos. Chem. Phys. Discuss., doi:10.5194/acp-2017-344, 2017
Manuscript under review for journal Atmos. Chem. Phys.
Discussion started: 26 April 2017

Atmospheric Chemistry and Physics Discussions

3. Results and discussion

3.1 XCH_4 over the Indian region: View from GOSAT and ACTM simulations

This section presents an analysis of XCH_4 mixing ratios observed by GOSAT from Jan 2011 to Dec 2014 over the Indian region. We also use the model simulations of XCH_4 for same period by varying surface emissions. The total surface CH_4 flux optimized by the inverse analysis (Patra et al., 2016) for same period are used to elucidate the variability in XCH_4 mixing ratios in relation with surface fluxes. These data are averaged for three months to smooth out sporadic fluctuations and to enable the examination of seasonal variations. We characterize the seasonal mean from January to March as "Winter", April to June as "Spring", July to September as "Summer or the southwest summer monsoon" and October to December as "Autumn"; this nomenclature is maintained throughout the article. The broad features (latitudinal distributions, seasonal distributions etc.,) of simulated XCH_4 mixing ratios and emission fluxes for both emission scenarios (AGS and CTL) are almost similar to each other. Here we discuss the simulations and emission flux for AGS scenario only. Figure 1a-b show the observed XCH_4 variation for two seasons; Spring and Autumn. XCH_4 mixing ratios are lower during the spring seasons and higher during the autumn seasons. A strong latitudinal gradient in XCH_4 is observed between the Gangetic plains and remainder of India. XCH_4 mixing ratios show the highest value (~1880 ppb) over the IGP, eastern and northeast Indian regions. As shown in Figure 1c-d, ACTM simulations are able to reproduce the observed latitudinal and seasonal gradients; i.e., higher mixing ratios during the SW monsoon and autumn seasons and lower mixing ratios during the winter and spring seasons over the Indian region. The optimized total CH_4 flux shows the high emissions over the IGP region and northeast Indian regions (Figure 1e-f). Most elevated levels of XCH_4 are observed simultaneously with the higher emissions, suggesting a direct connection between enhanced XCH_4 and high surface emissions. However, this connection is not valid over all locations. For example, the emission flux has been observed as higher during the spring season than the autumn season over most of the Indian region. In contrast, higher levels of XCH_4 are observed during the autumn season as compared to the spring season. These inconsistencies give the hint of other factors, transport and chemistry, responsible for the XCH_4 distribution, apart from the emissions, over the Indian region.

To study the seasonal XCH_4 pattern in details, the Indian landmass was partitioned into eight regions: Northeast India (NEI), Eastern India (EI), Eastern IGP (EIGP), Western IGP (WIGP), Central India (CI), Arid India (AI), Western India (WI), Southern Peninsula (SP), and two surrounding oceanic regions, the Arabian Sea (AS) and Bay of Bengal (BOB) (Figure 2a). Regional divisions are made based on spatial patterns of emission and XCH_4 (Figure 1a-f), and our knowledge of seasonal meteorological conditions. Figure 2b-k shows ACTM - GOSAT comparisons of XCH_4 time series from Jan 2011 to Dec 2014 over the selected study regions. The climatological monthly mean of XCH_4 data used in Figure 2 is provided in the supplementary information (Figure S1). Observations are limited during the SW monsoon season due to GOSAT retrieval limitations under cloud cover. The model captures the salient features in the seasonal cycles at very high statistical

Atmos. Chem. Phys. Discuss., doi:10.5194/acp-2017-344, 2017
Manuscript under review for journal Atmos. Chem. Phys.
Discussion started: 26 April 2017

Atmospheric Chemistry and Physics Discussions

significance as indicated by the high correlation coefficients ($r > 0.6$) over the selected regions (refer to supplementary Table S1). As shown in Table S1, both tracers show, the highest correlation coefficients over SP region and cleaner oceanic regions of the AS and BOB. The high ACTM-GOSAT correlations for the low/no emission regions suggest that transport and chemistry are accurately modeled in ACTM. Although we do not have statistically significant number of observations for the SW monsoon period, the few GOSAT data that were also simulated by ACTM over most of the study regions show high concentrations. Based on these comparisons, we can assume that model simulations can be used to understand XCH_4 variability over the India region. We confirmed that the modeled time series averaged over different regions with and without sampling at GOSAT sampling locations match well ($r \sim 0.9$).

3.2 Seasonal cycle of XCH_4 and possible controlling factors

This section discusses the average (2011-2014) XCH_4 annual cycle measured by GOSAT over the study regions discussed in Figure 2. The ACTM simulations with varying surface emissions optimized by the global inverse analysis (Patra et al., 2016), are further used to elucidate the seasonal variation in XCH_4. To investigate the role of vertical atmospheric layers in the seasonal XCH_4 cycle, the atmospheric column is segregated into five layers according to sigma partial pressure, starting from the surface level ($\sigma_p = 1$) to top of the atmosphere ($\sigma_p = 0$) with an equal spacing of 0.2. The layers bounded by the boundaries between 1.0-0.8, 0.8-0.6, 0.6-0.4, 0.4-0.2, and 0.2-0.0 of sigma pressure are denoted by LT, MT1, MT2, UT and UA, respectively. The columnar CH_4 mixing ratios are calculated in each partial layer (denoted by X_pCH_4) using the same formula used for the calculations of XCH_4 provided in Section 2.2. The model data for the missing observations period are also used in the XCH_4 annual cycle to understand its complete behaviour. The climatology of optimized total CH_4 flux for the same period is used to understand the link of surface emission to XCH4. Figure 3 shows the climatology of total CH_4 flux, climatology of XCH_4 and X_pCH_4 from model and observation over three selected regions, EIGP, SP and AI. These regions have been selected because they show distinct XCH_4 seasonal cycles and the distinct factors responsible for them. The remaining regions follow almost similar patterns to these three regions and hence the following discussion will equally applicable for them as well. The figures for the remaining regions are available in the supplementary information (Figures S2, S3). Further, differences in the X_pCH_4, calculated at the same time as the maxima and minima of the seasonal XCH_4 cycle, are used to calculate the percentage contributions of respected partial columns in the seasonal amplitude of XCH_4 (Figure 4). All these values are estimated from ACTM simulations.

Over the EIGP region, the emission seasonality differs substantially between the CTL case and the AGS case (Figure 3g) due to differences in emissions from wetlands, rice paddies and biomass burning; other anthropogenic emissions do not contain seasonal variations (Patra et al., 2016). The CTL case shows the emission peak in August (3.63 g CH_4 m^{-2} $month^{-1}$), while the AGS case shows the emission peak (4.43 g CH_4 m^{-2} $month^{-1}$) two months earlier, in June. In the AGS simulation over the EIGP region (Figure 3f), XCH_4 shows a peak in June that corresponds to the peak emissions (Figure 3g). However, simulated XCH_4 remains nearly constant until September, which is unexpected behavior based on emission seasonality. The

Atmos. Chem. Phys. Discuss., doi:10.5194/acp-2017-344, 2017
Manuscript under review for journal Atmos. Chem. Phys.
Discussion started: 26 April 2017

Atmospheric Chemistry and Physics Discussions

CTL simulation shows the peak in September, while the CTL emission scenario shows peak in August. Both simulation cases having different emission scenarios show peaks in September, which suggests a contribution from another factor apart from the emissions. Further, the X_pCH_4 seasonal cycle in the LT region is only partly similar to the emission pattern and the total column values. X_pCH_4 in the LT region (Figure 3e) shows an enhancement from March to June in AGS case, which corresponds to emissions and XCH_4 patterns. The X_pCH4 in the MT2 and UT layers show elevated mixing ratios until September while the other layers and the emission cycle do not show such features. Hence, the upper tropospheric layers (MT2 and UT) contribute elevated XCH_4 levels from July to September over the EIGP region (Figure 3f). Further, the seasonal cycle amplitudes at different layers reveal that 40% of the seasonal enhancement in the observed XCH_4 can be attributed to surface emissions; only 40% of CH_4 is available in the lower troposphere below 600hPa, which is directly affected by the surface emissions (Figure 4). The remaining 60% in seasonal enhancement comes from layers above 600 hPa.

In contrast to EIGP, a notable difference is observed in the emission seasonal cycle and XCH_4 seasonal cycle over SP region. The XCH_4 seasonal cycle and emission seasonal cycle are observed incompatible to each other. Both emission scenarios show distinct seasonal pattern; AGS shows annual high emissions from April to September, while CTL shows annual high during August-September (Figure 3n). On the other hand, being simulated from distinct emissions scenarios having different seasonal cycles, the XCH_4 shows identical seasonal cycle corresponding to both emission scenarios: peak in October and broader low from May to September. This suggests that the seasonal cycle of XCH_4 neither follow the emission pattern, nor the timing of the emission peak over SP. The seasonal X_pCH4 cycle in the LT layer over SP shows seasonal pattern similar to XCH_4, except the peak shifts from October to November. Surface winds from May to September over SP are from the southern hemisphere, which effectively flushes the air with low CH_4 and pushes the polluted air masses from the south to the north India region (refer to supplementary Figure S4). Further, the distinct seasonal cycle of chemical loss is observed over the SP region (refer to supplementary Figure S5) compared to other study regions; the loss rate starts increasing from 6 ppb day^{-1} in January to 12 ppb day^{-1} in April, reaching a plateau from April to September (~12 ppb day^{-1}). These evidences clearly suggest that the combined effect of transport and chemistry causes the low XCH_4 values for the May-September period. The peaks in the upper layers (Figure 3k-h) in October and transport from polluted continental layer in the LT layer (refer to supplementary Figure S4) could together contribute to the seasonal XCH_4 peak over SP. Over the SP region, about 60% of the seasonal XCH_4 amplitude is attributed to layers below 600 hPa and remaining 40% results from the other layers (Figure 4). In summary, activities, dominated in the atmosphere below 600 hPa, govern most of the XCH_4 seasonal cycle over this region.

Over the AI region, the seasonal XCH_4 cycle is different from those of the EIGP and SI regions. At a first glance, it seems the XCH_4 simulations (Figure 3t) follow the emission pattern over the AI region (Figure 3u). However in contrast to other cases mentioned above, the X_pCH_4 in the LT layer (Figure 3s) that is mostly affected by surface emission, does not resemble

Atmos. Chem. Phys. Discuss., doi:10.5194/acp-2017-344, 2017
Manuscript under review for journal Atmos. Chem. Phys.
Discussion started: 26 April 2017

Atmospheric Chemistry and Physics Discussions

the seasonal XCH_4 pattern over the AI region. The X_pCH_4 in the LT layer (Figure 4s) decreases from Jan to August and increases until December. On the other hand, in XCH_4, a significant peak (~1896 ppb) is observed in August followed a decline afterward (Figure 3t). This is an outstanding example, indicating no linkage between surface emissions and XCH_4 in terms of seasonal peak. An enhancement in the mixing ratios of X_pCH_4 is explicitly observed from May to August in the MT2 and UT layers (Figure 3p-q) and from June to August in the UA layer (Figure 3o). In contrast to previous two regions, EIGP and SI, over the AI region, the seasonal XCH_4 variation in the LT and MT1 layers together contribute only about 12% to the XCH_4 seasonal cycle amplitude (Figure 4). The upper layers contribute the remaining 88% (Figure 3v). Hence, based on this analysis, we conclude that instead of surface emissions, the high CH_4 in the upper tropospheric layers lead to the seasonal XCH_4 peak in August over this region. Similarly, Figure 4, Figure S2 and Figure S3 indicate that more than 60% in the seasonal amplitude of XCH_4 comes below 600 hPa over the regions lying in the southern half part of India, while more than 50% comes above 600 hPa over the regions mostly lying in the northern half part of India.

3.3 Source of higher CH_4 in the upper troposphere

Using ACTM simulations, we have shown that the higher CH_4 levels in the upper tropospheric region (~400-200 hPa) during the monsoon season contribute significantly to enhanced XCH_4 values over the northern regions of India. The source of higher mixing ratios in the upper troposphere as discussed in previous section can be explained by vertical transport of the CH_4 emitted from the surface, because no chemical CH_4 source is present at this height. Figure 5a-d shows the latitudinal cross section of the convective transport rate (in ppb day^{-1}) along with height and vertical velocity (hPa s^{-1}) averaged over 83-93°E for different seasons in 2011 (the ACTM_AGS simulation case). The positive/negative values of convective transport rate and vertical velocity in Figure 5a-d indicate the gain/loss of mass and downward/upward motions, respectively. Rapid updrafts, as indicated by higher negative values of vertical velocity, of higher CH_4 surface emissions by deep convection during the monsoon season are aided by the local topography over the IGP region (north of 20°N and east of 79°E in the Indian region). These updrafts cause higher mixing ratios of CH_4 in the upper tropospheric region (Figure 5g). The surface CH_4 mixing ratios are dissipated at an average rate of ~10 ppb day^{-1} during Spring-Autumn seasons (Figure 5b-d), and accumulate in the upper troposphere height at a similar rate; peak accumulation height varies with season. The horizontal cross-section of CH_4 at 200 hPa and wind vectors is plotted in Figures 5i-l for understanding the spatial extent of uplifted CH_4-rich air over the Indian region. The CH_4-rich air mass in the upper troposphere (~200 hPa) is further encountered with the anticyclonic winds during the SW monsoon season, which trap CH_4 and leads to widespread enhancement covering South Asia, and extending through the East Asia (Figure 5k). As a result of this, higher levels of CH_4 at upper troposphere, are not only limited over the regions where intense surface sources exist, the regions where surface sources are not comparatively strong are also covered by the high levels of CH_4 and hence contribute in the seasonal peak of XCH_4. After the SW monsoon season, the high westerly jet breaks the upper tropospheric anticyclone and elevated levels shift southward (Figure 5l) and cause higher CH_4 mixing ratios over southern India during the autumn season. Thus the convective updraft of high-CH_4 air mass, followed by horizontal spreading over the larger area by anticyclonic circulation,

control the redistribution of high CH_4 concentrations over the upper tropospheric region of northern part of India during SW monsoon season and over southern peninsula at this height during the early autumn season.

Like in Section 3.2, previous studies also show a shift in XCH_4 seasonal peak from August to October as we move from northern to Southern India and the major cause was discussed on the basis of emission from two major agricultural seasons of Kharif (May to October) and Rabi (November to April) (Hayashida et al., 2013; Kavitha et al., 2016). However, the detailed analysis of emission and transport component suggests that apart from surface emissions, the shift in XCH_4 seasonal peak could explained by shifting of high CH_4 levels associated with the anticyclonic winds at upper tropospheric height from northern to southern Indian region, respectively.

4. Conclusions

The dry-air mole fractions of methane (XCH_4) measured by GHGs Observation SATellite (GOSAT) were closely analyzed here over India and the surrounding seas. The region of interest is divided in to 8 sub-regions, namely, Northeast India (NEI), Eastern India (EI), Eastern IGP (EIGP), Western IGP (WIGP), Central India (CI), Arid India (AI), Western India (WI), Southern Peninsula (SP), and two surrounding oceanic regions, the Arabian Sea (AS) and Bay of Bengal (BOB. The JAMSTEC's atmospheric chemistry-transport model (ACTM) of CH_4 and total surface flux optimized by the inverse analysis are used for bridging the transport and emission information to observed XCH_4 mixing ratios and address their roles in the annual cycle in detail. We have been observed that distinct spatial and temporal features of XCH_4 are not only governed by the heterogeneous surface emissions, but also due to complex atmospheric transport mechanisms caused by the seasonally varying monsoon. The seasonal XCH_4 patterns often show a fair correlation between emissions and XCH_4 over the regions residing in the northern half of India (north of 15^{o}N: NEI, EI, EIGP, WIGP, CI, WI, AI), which implies XCH_4 levels are closely associated with the distribution of emission sources. However, detailed analysis of transport and emission reveal that only less than 40% of seasonal enhancement in the observed XCH_4 can be attributed to surface emissions over these regions except AI, as only this amount of CH_4 enhancement is available in the lower troposphere (below 600 hPa), which is directly affected by the surface emissions. In fact, ~40-60% of the CH_4 enhancement is in the uplifted air mass between 600-200 hPa over these regions. In contrast, over semi-arid AI region, as much as ~88% contributions to the XCH_4 seasonal cycle amplitude come from above 600 hPa, and only ~12% are contributed by the atmosphere below 600 hPa. The primary cause of the higher contributions from above 600 hPa over the northern Indian region is the characteristic transportation mechanisms in the Asian monsoon regions. The persistent deep convection during the southwest (SW) monsoon season (June-August) causes strong updrafts of CH_4 from the surface to upper troposphere, which is then distributed by anticyclonic winds over the northern Indian region. These transport mechanisms caused the elevated CH_4 mixing ratios in the upper troposphere hence contributed significantly to the seasonal peak in XCH_4 over northern India. In contrast to these regions, over the SP region, the major contributions (about 60%) to XCH_4 seasonal amplitude come from the lower atmosphere (~1000-600 hPa). Both transport and chemistry dominate in the lower atmosphere over SP region and,

as a result of it, the seasonal variation of XCH_4 is not corresponding to the seasonality of the local emissions. As upper level anticyclones do not cover the southern Indian region in its active phase during the SW monsoon season, the enhancement in XCH_4 is not observed over the southern peninsular region during the SW monsoon season.

Most satellite sensors are designed to provide total columnar observations of atmospheric chemical species. This study opens a new window for interpreting columnar measurements for surface emissions of greenhouse gases particularly over the Asian monsoon region where characteristic meteorology dominates, and should aid users in carefully applying scientific data in the future to not draw erroneous conclusions.

Acknowledgements

The Environment Research and Technology Development Fund (A2-1502) of the Ministry of the Environment, Japan, supported this research. The data used for preparing the figures, and table could be available on request. The corresponding author may be contacted for the same.

References

Baker, A. K., Schuck, T. J., Brenninkmeijer, C. A. M., Rauthe-Schöch, A., Slemr, F., van Velthoven, P. F. J., and Lelieveld, J.: Estimating the contribution of monsoon-related biogenic production to methane emissions from South Asia using CARIBIC observations, Geophys. Res. Lett., 39, L10813, doi:10.1029/2012GL051756, 2012.

Crutzen. P.J., Aselmann, I., and Seiler, W.: Methane production by domestic animals, wild ruminants other herbivorous fauna and humans. Tellus 38B, 271-284, doi:10.1111/j.1600-0889.1986.tb00193.x, 1986.

Cao, M., Gregson, K., and Marshall, S.: Global methane emission from wetlands and its sensitivity to climate change. Atmos. Environ. 32 (19), 3293-3299, doi:10.1016/S1352-2310 (98) 00105-8, 1998.

Chandra, N., Venkataramani, S., Lal, S., Sheel, V. & Pozzer, A.: Effects of convection and long-range transport on the distribution of carbon monoxide in the troposphere over India. Atmospheric Pollution Research 7, 775 – 785, doi:10.1016/j.apr.2016.03.005, 2016.

Dlugokencky, E. J., Nisbet, E. G., Fisher, R., and Lowry, D.: Global atmospheric methane: Budget, changes, and dangers, Philos. Trans. R. Soc. London, Ser. A., 369, 2058–2072, 2011.

EDGAR42FT, 2013: Global emissions EDGAR v4.2FT2010 (October 2013). [Available at http://edgar.jrc.ec.europa.eu/overview.php?v=42FT2010.].

Fung, I., John, J., Lerner, J., Matthews, E., Prather, M., Steele, L. P., and Fraser, P. J.: Three-dimensional model synthesis of the global methane cycle, J. Geophys. Res., 96, 13033–13065, doi:10.1029/91JD01247, 1991

Frankenberg, C., Meirink, J. F., van Weele, M., Platt, U., and Wagner, T.: Assessing methane emissions from global space-borne observations, Science, 308, 1010–1014, 2005.

Frankenberg, C., Meirink, J.F., Bergamaschi, P., Goede, A.P.H., Heimann, M., Korner, S., Platt, U., Weele, M. V., and

Wagner, T.: Satellite chartography of atmospheric methane from SCIAMACHY onboard ENVISAT: Analysis of the years 2003 and 2004, J. Geophys. Res.,111, D07303, doi:10.1029/2005JD006235, 2006.

Hayashida, S., Ono, A., Yoshizaki, S., Frankenberg, C., Takeuchi, W., Yan, X.: Methane concentrations over Monsoon Asia as observed by SCIAMACHY: Signals of methane emission from rice cultivation. Remote Sensing of Environment 139, 246–256, doi: 10.1016/j.rse.2013.08.008, 2013.

Kuze, A., Suto, H., Nakajima, M., and Hamazaki, T.: Thermal and near infrared sensor for carbon observation Fourier transform spectrometer on the Greenhouse Gases Observing Satellite for greenhouse gases monitoring. Appl. Opt. 48, 6716–6733, doi: 10.1364/AO.48.006716, 2009.

Kar, J., Deeter, M. N., Fishman, J., Liu, Z., Omar, A., Creilson, J. K., Trepte, C. R., Vaughan, M. A., and Winker, D. M.: Wintertime pollution over the Eastern Indo-Gangetic Plains as observed from MOPITT, CALIPSO and tropospheric ozone residual data, Atmos. Chem. Phys., 10, 12273-12283, doi:10.5194/acp-10-12273-2010, 2010.

Kavitha, M. and Nair, P. R.: Region-dependent seasonal pattern of methane over Indian region as observed by SCIAMACHY. Atmospheric Environment 131, 316–325, doi:10.1016/j.atmosenv.2016.02.008, 2016.

Lal, S., Venkataramani, S., Chandra, N., Cooper, O. R., Brioude, J., and Naja, M.: Transport effects on the vertical distribution of tropospheric ozone over western India, J. Geophys. Res. Atmos., 119, 10,012–10,026, doi:10.1002/2014JD021854, 2014.

Minami, K., and Neue, H. U.: Rice paddies as a methane source. Clim. Change Lett.27, 13-26, doi:10.1007/BF01098470, 1994.

Morino, I., Uchino, O., Inoue, M., Yoshida, Y., Yokota, T., Wennberg, P. O., Toon, G. C., Wunch, D., Roehl, C. M., Notholt, J., Warneke, T., Messerschmidt, J., Griffith, D. W. T., Deutscher, N. M., Sherlock, V., Connor, B., Robinson, J., Sussmann, R., and Rettinger, M.: Preliminary validation of column-average volume mixing ratios of carbon dioxide and methane retrieved from GOSAT short-wavelength infrared spectra. Atmos. Meas. Tech., 4, 1061−1076, doi:10.5194/amt-4-1061-2011, 2011.

Myhre, G., Shindell, D., Bréon, F.-M., Collins, W. Fuglestvedt, J., Huang, J., Koch, D. Lamarque, J.-F., Lee, D., Mendoza, B., Nakajima, T., Robock, A., Stephens, G. Takemura, T., and Zhang, H.: Anthropogenic and natural radiative forcing, in: Climate Change 2013: The Physical Science Basis, Fifth Assessment Report of the Intergovernmental Panel on Climate Change, edited by: Stocker, T. F. et al., Cambridge University Press, Cambridge, UK, New York, NY, USA, 659–740, 2013.

Olivier, J. G. J., Aardenne, J.A.V., Dentener, F., Ganzeveld, L. N., Peters, J.A.H.W.:Recent trends in global greenhouse Gas emissions: Regional trends and spatial distribution of key sources, in: Non-CO_2 Greenhouse Gases (NCGG-4), edited by: van Amstel, A., 325–330, Millpress, Rotterdam, Netherlands, 2005.

Onogi, K., Tsutsui, J., Koide, H., Sakamoto, M., Kobayashi, S., Hatsushika, H. Matsumoto, T., Yamazaki, N., Kamahori, H., Takahashi, K., Kadokura, S., Wada, K., Kato, K., Oyama, R., Ose, T., Mannoji, N., and Taira, R.: The JRA-25 reanalysis, J. Meteorol. Soc. Jpn., 85, 369–432, 2007.

405 Olsen, K. S., Strong, K., Walker, K. A., Boone, C. D., Raspollini, P., Plieninger, J., Bader, W., Conway, S., Grutter, M., Hannigan, J. W., Hase, F., Jones, N., de Mazière, M., Notholt, J., Schneider, M., Smale, D., Sussmann, R., and Saitoh, N.: Comparison of the GOSAT TANSO-FTS TIR CH_4 volume mixing ratio vertical profiles with those measured by ACE-FTS, ESA MIPAS, IMK-IAA MIPAS, and 16 NDACC stations, Atmos. Meas. Tech. Discuss., doi:10.5194/amt-2017-6, in review, 2017.

410 Park, M., Randel, W. J., Kinnison, D. E., Garcia, R. R., and Choi, W.: Seasonal variation of methane, water vapor, and nitrogen oxides near the tropopause: Satellite observations and model simulations. Journal of Geophysical Research: Atmospheres 109, doi: 10.1029/2003JD003706. D03302, 2004.

Patra, P. K., Takigawa, M., Ishijima, K., Choi, B. C., Cunnold, D., Dlugokencky, E. J., Fraser, P., A. J., Gomez-Pelaez, Goo, T. Y., Kim, J. S., Krummel, P., Langenfelds, R., Meinhardt, F., Mukai, H., O'Doherty, S., Prinn, R. G., Simmonds,

415 P., Steele, P., Tohjima, Y., Tsuboi, K., Uhse, K., Weiss, R., Worthy, D., and Nakazawa, T.: Growth rate, seasonal, synoptic, diurnal variations and budget of methane in lower atmosphere, J. Meteorol. Soc. Jpn., 87(4), 635-663, doi: 10.2151/jmsj.87.635, 2009.

Patra, P. K., Houweling, S., Krol, M., Bousquet, P., Belikov, D., Bergmann, D., Bian, H., Cameron-Smith, P., Chipperfield, M. P., Corbin, K., Fortems-Cheiney, A., Fraser, A., Gloor, E., Hess, P., Ito, A., Kawa, S. R., Law, R. M.,

420 Loh, Z., Maksyutov, S., Meng, L., Palmer, P. I., Prinn, R. G., Rigby, M., Saito, R., and Wilson, C.: TransCom model simulations of CH_4 and related species: Linking transport, surface flux and chemical loss with CH4 variability in the troposphere and lower stratosphere, Atmos. Chem. Phys., 11, 12,813–12,837, doi:10.5194/acp-11-12813-2011, 2011.

Patra, P. K., Krol, M. C., Montzka, S. A., Arnold, T., Atlas, E. L., Lintner, B. R., Stephens, B. B., Xiang, B., Elkins, J. W., Fraser, P. J., Ghosh, A., Hintsa, E. J., Hurst, D. F., Ishijima, K., Krummel, P. B., Miller, B. R., Miyazaki, K.,

425 Moore, F. L., Mühle, J., O'Doherty, S., Prinn, R. G., Steele, L. P., Takigawa, M., Wang, H. J., Weiss, R. F., Wofsy, S. C., and Young, D.: Observational evidence for interhemispheric hydroxyl parity, Nature, 513, 219–223, 2014.

Patra, P. K., Saeki, T., Dlugokencky, E. J., Ishijima, K., Umezawa, 5 T., Ito, A., Aoki, S., Morimoto, S., Kort, E. A., Crotwell, A., Kumar, R., and Nakazawa, T.: Regional methane emission estimation based on observed atmospheric concentrations (2002–2012), J. Meteorol. Soc. Jpn., 94(1), 91–113, doi:10.2151/jmsj.2016-006, 2016.

430 Rao, Y. P.: Southwest monsoon: Synoptic Meteorology, Meteor. Monogr., No. 1/1976, India Meteorological Department, 367 pp, 1976.

Randel, W. J. and Park, M.: Deep convective influence on the Asian summer monsoon anticyclone and associated tracer variability observed with Atmospheric Infrared Sounder (AIRS). J. Geophys. Res. 111, doi: 10.1029/2005JD006490, 2006.

435 Sugimoto, A., Inoue, T., Kirtibutr, N. and Abe, T.: Methane oxidation by termite mounds estimated by the carbon isotopic composition of methane. Glob. Biogeochem. Cycles 12 (4), 595-605, doi:10.1029/98GB02266, 1998.

Shindell, D. T., Faluvegi, G., Koch, D. M., Schmidt, G. A., Unger, N., Bauer, S. E.: Improved attribution of climate forcing to emissions, Science, 326, 716-718, doi: 10.1126/science.1174760, 2009.

Schuck, T. J., Ishijima, K., Patra, P. K., Baker, A. K., Machida, T., Matsueda, H., Sawa, Y., Umezawa, T., Brenninkmeijer, C. A. M., and Lelieveld, J.: Distribution of methane in the tropical upper troposphere measured by CARIBIC and CONTRAIL aircraft, J. Geophys. Res.,117, D19304, doi:10.1029/2012JD018199, 2012.

Spivakovsky, C. M., Logan, J. A., Montzka, S. A., Balkanski, Y. J., Foreman-Fowler, M., Jones, D. B. A., Horowitz, L. W., Fusco, A. C., Brenninkmeijer, C. A. M., Prather, M. J., Wofsy, S. C., and McElroy, M. B.: Three-dimensional climatological distribution of tropospheric OH: update and evaluation, J. Geophys. Res., 105, 8931–8980, doi:10.1029/1999JD901006, 2000.

Worden, J. R., Turner, A. J., Bloom, A., Kulawik, S. S., Liu, J., Lee, M., Weidner, R., Bowman, K., Frankenberg, C., Parker, R., and Payne, V. H.: Quantifying lower tropospheric methane concentrations using GOSAT near-IR and TES thermal IR measurements, Atmos. Meas. Tech., 8, 3433-3445, doi:10.5194/amt-8-3433-2015, 2015.

Xiong, X., Houweling, S., Wei, J., Maddy, E., Sun, F., and Barnet, C.: Methane plume over south Asia during the monsoon season: satellite observation and model simulation, Atmos. Chem. Phys., 9, 783-794, doi:10.5194/acp-9-783-2009, 2009.

Yoshida, Y., Kikuchi, N., Morino, I., Uchino, O., Oshchepkov, S., Bril, A., Saeki, T., Schutgens, N., Toon, G. C., Wunch, D., Roehl, C. M., Wennberg, P. O., Griffith, D. W. T., Deutscher, N. M.,Warneke, T., Notholt, J., Robinson, J., Sherlock, V., Connor, B., Rettinger, M., Sussmann, R., Ahonen, P., Heikkinen, P., Kyrö, E., Mendonca, J., Strong, K., Hase, F., Dohe, S., and Yokota,T.: Improvement of the retrieval algorithm for GOSAT SWIRXCO$_2$ and XCH$_4$ and their validation using TCCON data, Atmos. Meas. Tech., 6, 1533–1547, doi:10.5194/amt-6-1533-2013, 2013.

Yan, X., Akiyama, H., Yagi, K., and Akimoto, H.: Global estimations of the inventory and mitigation potential of methane emissions from rice cultivation conducted using the 2006 Intergovernmental Panel on Climate Change Guidelines, Global Biogeochem. Cycles, 23, GB2002, doi:10.1029/2008GB003299.

Zou, M., Xiong, X., Saitoh, N., Warner, J., Zhang, Y., Chen, L., Weng, F., and Fan, M.: Satellite observation of atmospheric methane: intercomparison between AIRS and GOSAT TANSO-FTS retrievals, Atmos. Meas. Tech., 9, 3567-3576, doi:10.5194/amt-9-3567-2016, 2016.

Atmos. Chem. Phys. Discuss., doi:10.5194/acp-2017-344, 2017
Manuscript under review for journal Atmos. Chem. Phys.
Discussion started: 26 April 2017

Atmospheric Chemistry and Physics Discussions

Figures.

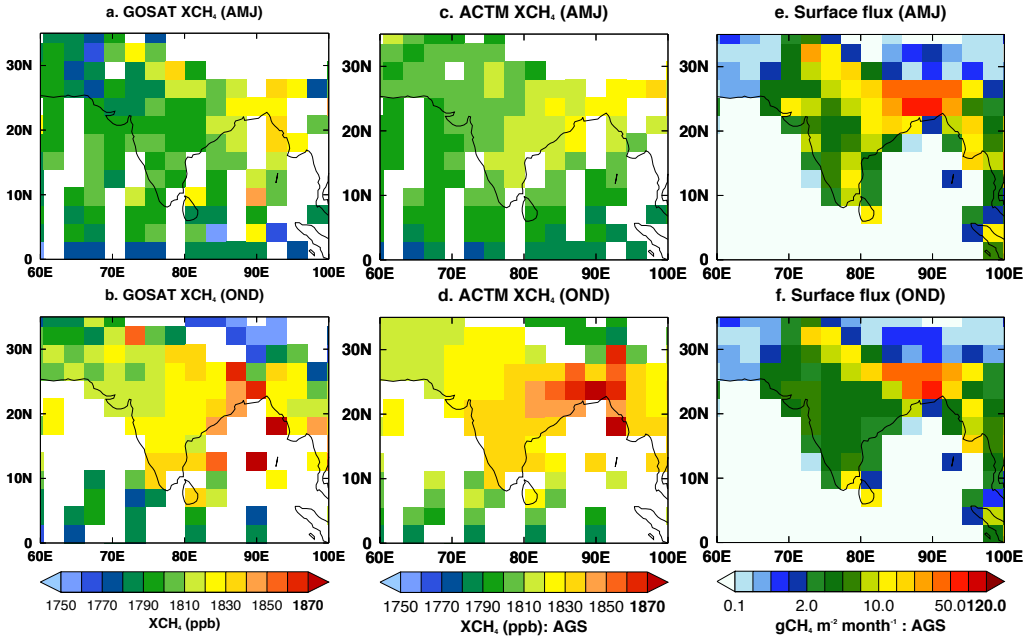

Figure 1: Average seasonal distributions (from 2011 to 2014) of XCH_4 obtained from GOSAT observations (a-b), ACTM simulations (c-d) and CH_4 emission consisting of all the natural and anthropogenic emissions (e-f: ACTM_AGS case) over the Indian region. Optimized emissions are shown from a global inversion of surface CH_4 concentrations (Patra et al., 2016) and multiplied by a constant factor of 12 for a clear visualization. The ACTM is first sampled at the location and time of GOSAT observations and then seasonally averaged. The white spaces in panels (a-d) are due to the missing data caused by satellite retrieval limitations from cloud cover.

Atmos. Chem. Phys. Discuss., doi:10.5194/acp-2017-344, 2017
Manuscript under review for journal Atmos. Chem. Phys.
Discussion started: 26 April 2017

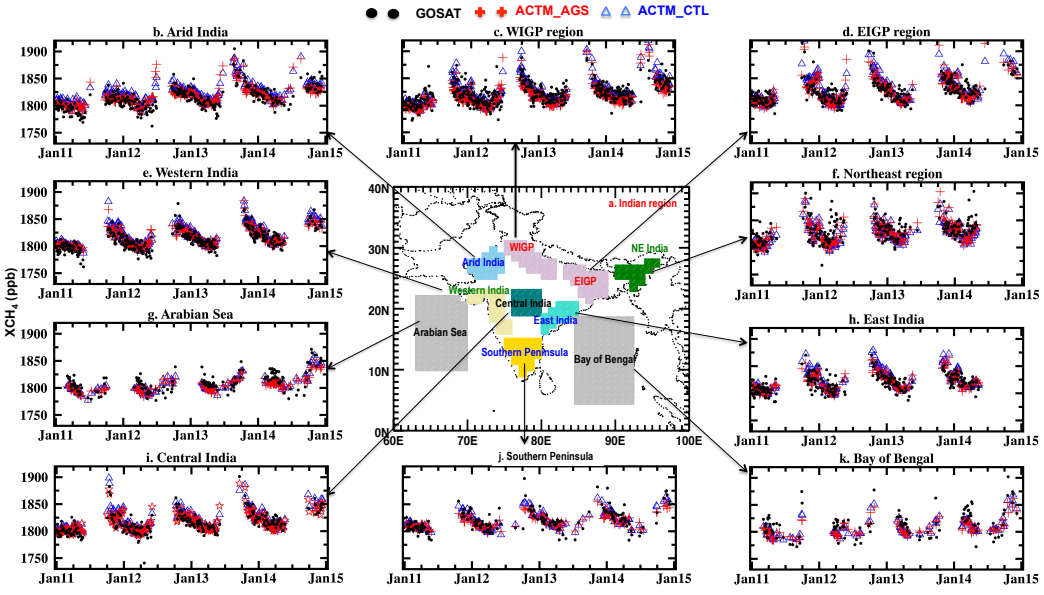

Figure 2: (a) The map of the regional divisions (shaded) for the time series analysis. (b-l) Time series of XCH_4 over the selected regions (shown in map) as obtained from GOSAT and simulated by ACTM for two different emission scenarios, namely, ACTM_AGS and ACTM_CTL. The gaps are due to the missing observational data.

Atmos. Chem. Phys. Discuss., doi:10.5194/acp-2017-344, 2017
Manuscript under review for journal Atmos. Chem. Phys.
Discussion started: 26 April 2017

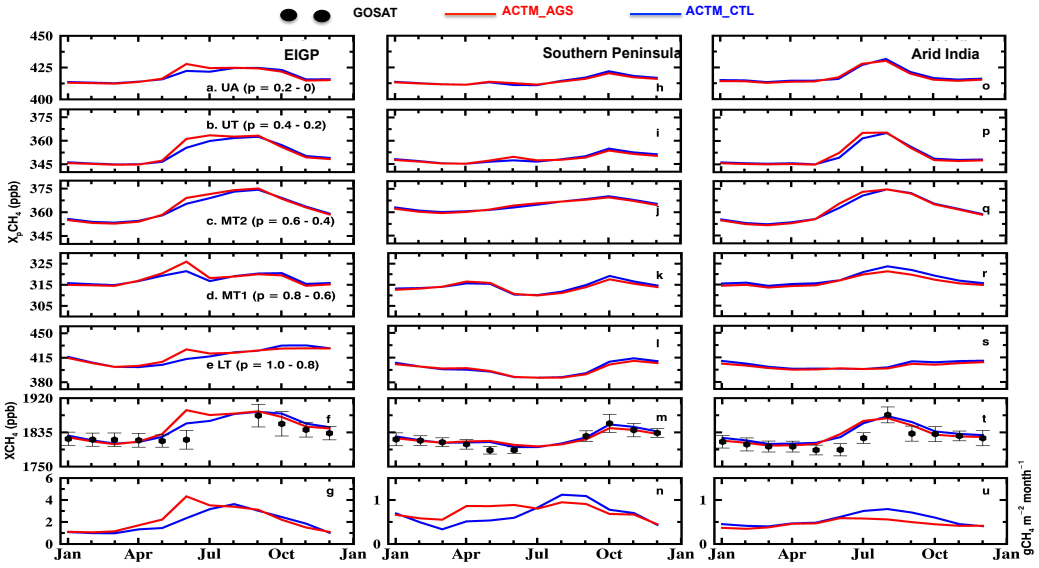

495 Figure 3: The bottom panels show the monthly mean climatology of the total optimized CH_4 emissions (panels g, n, u); estimated after performing the global inverse analysis (Patra et al., 2016). The second bottom panels show XCH_4 obtained from the GOSAT observations (black circles in panels f, m, t) and ACTM simulations (panels f, m, t) over the Eastern IGP (first column), Southern Peninsula (second column) and Arid India region (third column). Monthly climatology is based on the monthly mean values for the period of 2011-2014 for all the values. The error bars in the GOSAT monthly mean values
500 depict the 1-sigma standard deviations for the corresponding months (f, m, t). The 1-sigma values are not plotted for the model simulations to maintain figure clarity. Simulations are based on two different emission scenarios namely ACTM_CTL (blue lines) and ACTM_AGS (red lines) based on the different combinations of emissions. The upper five panels show the monthly climatology of partial columnar methane (denoted by x_pCH_4) calculated at five different partial sigma-pressure layers; 1.0-0.8 (e, l, s), 0.8-0.6 (d, k, r), 0.6-0.4 (c, j, q), 0.4-0.2 (b, I, p) and 0.2-0.0 (a, h, n). Please note that the y scales in
505 the emission plots over southern peninsula and Arid India (n and u) are different than over the EIGP region (g).

Atmos. Chem. Phys. Discuss., doi:10.5194/acp-2017-344, 2017
Manuscript under review for journal Atmos. Chem. Phys.
Discussion started: 26 April 2017

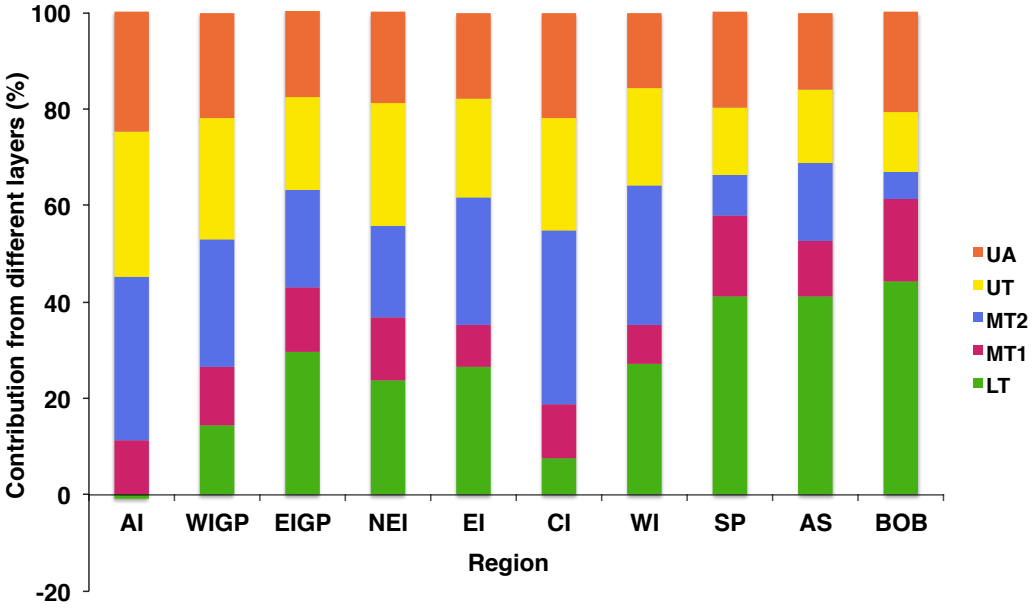

Figure 4: Contributions of partial columns in the seasonal amplitude of XCH_4 over selected regions for AGS case. Differences in the X_pCH_4, calculated at the same time as the maxima and minima of the seasonal XCH_4 cycle, are used to calculate the percentage contributions of respected partial columns in the seasonal amplitude of XCH_4.

Atmos. Chem. Phys. Discuss., doi:10.5194/acp-2017-344, 2017
Manuscript under review for journal Atmos. Chem. Phys.
Discussion started: 26 April 2017

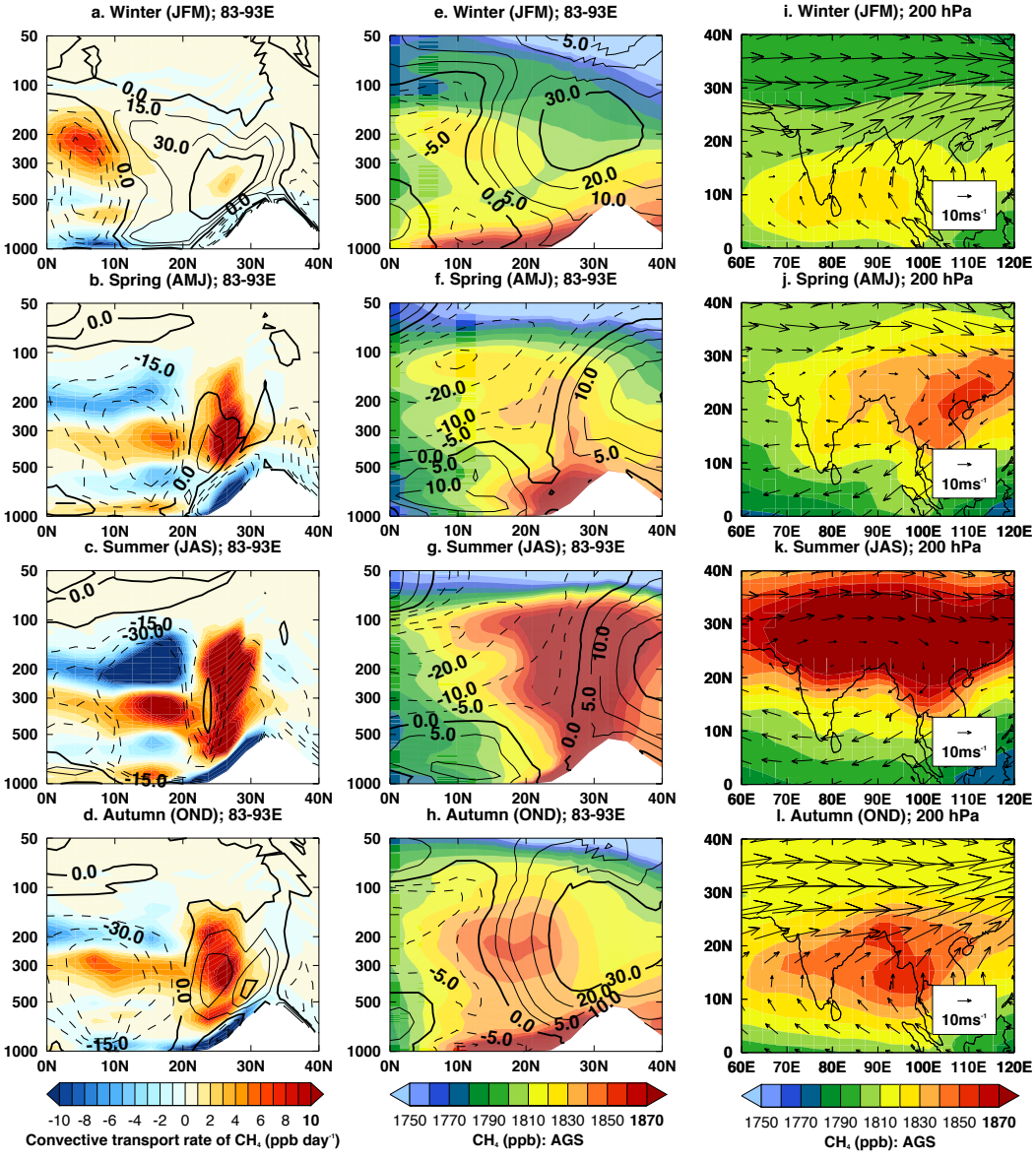

515 **Figure 5:** Vertical structure of seasonally averaged CH_4 transport rate due to the convection (a-d, in ppb day^{-1}) and CH_4 mixing ratios (e-h from AGS scenarios) averaged over 83-93°E for the year of 2011. Positive and negative transport rate

Atmos. Chem. Phys. Discuss., doi:10.5194/acp-2017-344, 2017
Manuscript under review for journal Atmos. Chem. Phys.
Discussion started: 26 April 2017

Atmospheric Chemistry and Physics Discussions

values represent the accumulation and dissipation of mass, respectively. The contour lines in the fist (a-d) and second (e-h) columns depict the average omega velocity (in hPa s^{-1}) and u wind component, respectively for the same period. The solid contour lines show the positive values and dotted lines show negative values. Positive and negative values of the omega velocity represent downward and upward motions, respectively. The zero value of u wind shows wind is pure either southerly or northerly. White spaces in zonal-mean plots (a- h) show the missing data due to orography. The rightmost column depicts the maps of averaged CH_4 and wind vectors (in m s^{-1}; arrow) during all the four seasons in 2011 at 200 hPa height (i-l).